Inorganic Chemistry

Article

pubs.acs.org/IC

Cationic Cryptand Complexes of Tin(II)

Jessica C. Avery,[†] Margaret A. Hanson,[†] Rolfe H. Herber,*[,‡] Kamila J. Bladek,[†] Paul A. Rupar,[†] Israel Nowik,[‡] Yining Huang,*[,†] and Kim M. Baines*[,†]

[†]Department of Chemistry, University of Western Ontario, London, Ontario, Canada N6A 5B7

[‡]Racah Institute of Physics, The Hebrew University of Jerusalem, 91904 Jerusalem, Israel

Supporting Information

ABSTRACT: A series of cationic cryptand complexes of tin(II), [Cryptand[2.2.2]SnX][SnX_3] (**10**, X = Cl; **11**, X = Br; **12**, X = I) and [Cryptand[2.2.2]Sn][$OTf]_2$ (**13**), were synthesized by the addition of cryptand[2.2.2] to a solution of either tin(II) chloride, iodide, or trifluoromethanesulfonate. The complexes could also be synthesized by the addition of the appropriate trimethylsilyl halide (or pseudohalide) reagent to a solution of tin(II) chloride and cryptand[2.2.2]. The complexes were characterized using a variety of techniques including NMR, Raman, and temperature-dependent Mössbauer spectroscopy, mass spectrometry, and X-ray diffraction.

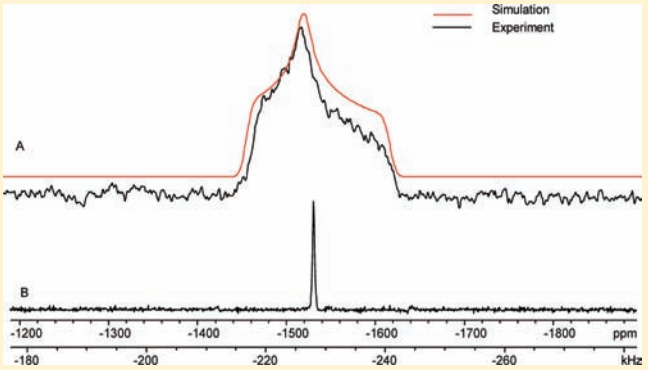

1. INTRODUCTION

The synthesis of stable, heavier group 14 cations in the condensed phase has been a formidable and exciting challenge.[1−7] After decades of intense research, the community now understands the important factors necessary to produce stable cations in the +4 oxidation state in the condensed phase and free from the influence of donors: bulky substituents, nonnucleophilic solvents and/or weakly coordinating anions are the essential design features. In contrast, cations with the group 14 element in the +2 oxidation state have received much less attention. Like cations in the +4 oxidation state, they require stabilization in some form, and in this case, stabilization by electron-donating species such as N-heterocyclic carbenes,[8] cyclopentadienyl-based ligands[9−11] or N-donating ligands,[12,13] is prevalent.

Cyclic polyethers, such as cryptands and crown ethers, have been used to complex metal cations across the entire periodic table. Polyethers have long been known to complex metallic tin and lead in the +2 oxidation state. More recently, it has been demonstrated that the multiple weak interactions with the heteroatoms of a polyether can also stabilize nonmetals including germanium and silicon in group 14.[14] In 2008, our group reported the first example of a germanium(II) dication (**1**)[15] encapsulated within cryptand[2.2.2], where the macrocyclic ether provides stabilization and protection for the reactive species. Our group, in collaboration with Macdonald,[16] also synthesized and structurally characterized Ge(II) mono- and dications (**2**, **3**, **4**) complexed by crown ethers of various sizes (Chart 1). The differences in the observed structures of the cationic complexes are related to the size of the cavity of the crown ether, and hence, its ability to encapsulate the atom. If the cavity is small, a sandwich type complex is formed;

Chart 1. Macrocyclic Polyether Ge and Sn Complexes[a]

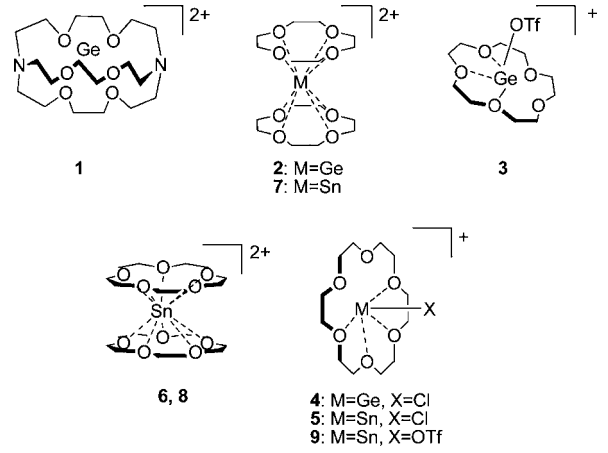

[a]Counterions: **1**: TfO^-; **2**: TfO^- or $GeCl_3^-$; **3**: TfO^-; **4**: $GeCl_3^-$; **5**: $SnCl_3^-$; **6**: $SnCl_3^-$; **7**: TfO^-; **8**: TfO^-; **9**: TfO^-.

however, as the size of the crown ether cavity increases, encapsulation is observed. Reid and co-workers have isolated germanium cationic complexes with aza- and mixed thia-oxa macrocycles, indicating that nitrogen and sulfur are also suitable donors for the stabilization of these reactive species.[17] Lead(II) complexes with cryptand[2.2.2], forming mono- or dicationic structures where the lead is encapsulated within the cavity of the cryptand. In addition to interacting with the eight heteroatoms of the cryptand, water and/or the perchlorate

Received: March 30, 2012
Published: June 11, 2012

   dx.doi.org/10.1021/ic3006713 | *Inorg. Chem.* 2012, 51, 7306−7316

Scheme 1

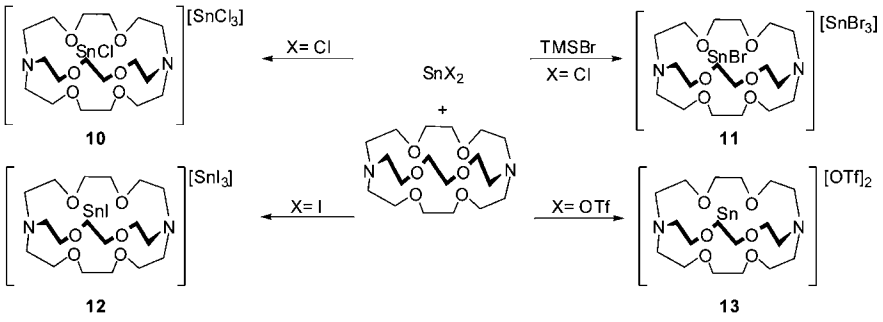

anion also coordinate to the metal cation.[18,19] Recently, Si(II) has been shown to complex with 12-crown-4 during the degradation of cyclic polyethers, using $(Me_5C_5)Si^+$ as the silicon source and catalyst.[20]

Tin(II) crown ether complexes were first studied in the group of Herber.[21,22] Mössbauer spectroscopy was used to elucidate the structure and determine the nature of the stereochemically active lone pair on tin. Crown ether complexes of tin(II) halides, [(18-crown-6)SnCl][$SnCl_3$] (**5**) and [$(15\text{-crown-5})_2$Sn][$SnCl_3$]$_2$ (**6**) were structurally characterized by X-ray diffraction several years later by Nicholson and co-workers, confirming Herber's original structural assignment (Chart 1).[23,24] Recently, polyether complexes of tin(II) cations have been revisited by Macdonald and co-workers, who reported the synthesis and structural characterization of tin(II) complexes[25a] of 12-crown-4 (**7**), 15-crown-5 (**8**), and 18-crown-6 (**9**) and glyme-like podand ligands[25b] with triflate as the counterion (Chart 1). The structure of each crown ether complex is dependent on the size of the ring, consistent with Nicholson's observations. A tethered crown ether complexed to a tin(IV) cation[26a] in addition to a mixed valent tin crown ether complex[26b] have also been reported. Although the synthesis of a variety of tin(II) crown ether complexes has been achieved, surprisingly the synthesis of cryptand complexes of tin(II) has not yet been examined. We now report on the synthesis and characterization of the first tin(II) complexes with cryptand[2.2.2] and compare the structure and bonding of these complexes to those with crown ethers.

2. RESULTS AND DISCUSSION

2.1. Halide Complexes. Cryptand[2.2.2] was added to a solution of tin dichloride in tetrahydrofuran (THF) (Scheme 1). A white solid rapidly precipitated from the clear, colorless solution. The solid was characterized by NMR, Raman and Mössbauer spectroscopy, electrospray ionization (ESI)-mass spectrometry (ESI-MS) and single crystal X-ray diffraction, and identified as [Cryptand[2.2.2]SnCl][$SnCl_3$] (**10**). The bromide (**11**) derivative was synthesized by the addition of trimethylsilyl bromide to the reaction mixture. Complex **12** is accessible by the addition of cryptand[2.2.2] to a solution of anhydrous SnI_2.

For each derivative, the ESI-MS spectrum revealed a mass cluster with the appropriate isotopic pattern for tin. The chloride derivative (**10**) revealed a mass cluster with a mass to charge (m/z) ratio centered at m/z 531 corresponding to $^{12}C_{18}{}^{1}H_{36}{}^{14}N_2{}^{16}O_6{}^{120}Sn^{35}Cl$, a cation containing cryptand, tin, and chlorine. Each peak is separated by one m/z unit indicating a singly charged species. The bromide (**11**) and iodide (**12**) derivatives revealed mass clusters centered at m/z 573 and m/z 623, respectively, corresponding to cations containing cryptand, tin and the appropriate halide. There was no evidence of multiply charged species in any of the mass spectra of **10**–**12**.

The FT-Raman spectra of **10** and **11** exhibit absorptions (293, 259, 136, and 111 cm^{-1} for **10** and 202, 182, and 86 cm^{-1} for **11**) consistent with a trihalostannate anion, SnX_3^- (X = Cl for **10** and X = Br for **11**), identifying the counterion in the complexes.[27] In **11**, complete halogen exchange occurred. The Raman spectrum of **12** (Supporting Information, Figure S1) does not contain signals consistent with the triodidostannate anion (162, 148, 61, 48 cm^{-1}).[27,28] A broad absorption at 133 cm^{-1} was observed. In contrast, the ESI-MS negative mode spectrum of **12** reveals a prominent mass cluster centered at m/z 500 that does correspond to SnI_3^-. We attribute the broad signal in the Raman spectrum to an overlap of signals corresponding to the Sn–I bond of the triodidostannate anion and the cation. All other absorptions in the Raman spectrum of **12** are comparable to those of **10** and **11**.

Single crystals suitable for X-ray diffraction were grown by slow diffusion of diethyl ether into a concentrated solution of THF for **10** and **11**. The two crystals are isomorphic. The X-ray data of **10** reveal two moieties within the formula unit: a tin-chloride moiety complexed by cryptand[2.2.2] and tin trichloride to give [Cryptand[2.2.2]SnCl][$SnCl_3$] (Figure 1). Selected bond lengths are listed in Table 1. The Sn–Cl distances of 2.452(3), 2.474(2), and 2.474(2) Å in the counterion, $SnCl_3^-$, were consistent with reported values.[23] The anion shows no interaction with the cationic moiety based on the long tin–tin distance of 7.399(1) Å and the cationic tin-

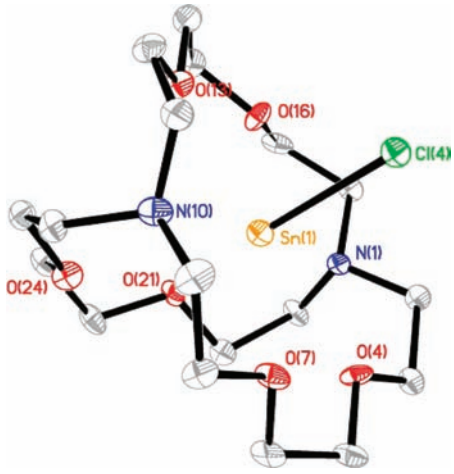

Figure 1. Thermal ellipsoid plot (30% probability surface) of 10^+. The counterion, $SnCl_3^-$, has been removed for clarity. Selected bond lengths are given in Table 1.

dx.doi.org/10.1021/ic3006713 | Inorg. Chem. 2012, 51, 7306–7316

Table 1. Selected Bond Lengths in Å for 10, 11, and 13[a]

compound	**10**, X = Cl	**11**, X = Br	**13**, X = O (triflate)
Sn−X	cation: 2.532(2)	cation: 2.6879(11)	*1*: 5.062(4), 5.383(5)
	anion: 2.474(2), 2.452(3), 2.474(2)	anion: 2.6238(11), 2.6058(11), 2.6178(10)	*2*: 2.698(5), 6.094(4)
Sn−O (cryptand)	2.745(6), 3.000(7), 2.613(6), 2.709(6), 2.876(6), 3.076(6)	2.709(6), 2.624(5), 3.020(5), 2.870(4), 2.970(5), 2.769(6)	*1*: 2.508(3), 2.734(4), 2.711(4), 2.456(3), 2.644(4), 2.697(4)
			2: 2.530(3), 2.580(5), 2.783(4), 2.596(3), 2.782(5), 2.61(2)
Sn−N	2.740(7), 2.968(9)	2.781(6), 2.952(6)	*1*: 2.832(4), 2.749(4)
			2: 2.707(4), 2.862(4)

[a]The two tin cations in **13** have been differentiated as *1* and *2*.

Table 2. Hyperfine Parameters and Associated Values Extracted from the ^{119}Sn Mössbauer Data and X-ray Data for 10, 11, and 13

	10		**11**		**13**	
parameters	cation	anion	cation	anion	cation	units
IS(90 K)	4.32(3)	2.92(6)	4.21(2)	3.22(4)	4.40(1)	mm sec^{-1}
QS(90 K)	1.13(3)	0.93(13)	1.19(2)	1.18(4)	0.60(1)	mm sec^{-1}
$-\mathrm{d}\ln A/\mathrm{d}T$	18.9(2)	26.3(14)	16.8(15)	24.0(16)	17.5(6)	K^{-1} × 10^{-3}
$k^2\langle x_{ave}^2\rangle_{M,150}$	2.83(4)	3.87(4)	2.54(14)	3.73(14)	2.63(9)	
$k^2\langle x_{ave}^2\rangle_{X,150}$	4.86(4)	3.84(4)	3.01(9)	4.16(8)	2.63(3)	

anionic chloride distances averaging 6.479(5) Å. The tin atom, complexed within the cavity of cryptand[2.2.2], is bonded to a chloride anion at a distance of 2.532(2) Å, which is within the sum of ionic radii for tin(II) dication and a chloride anion (1.12 and 1.67 Å, respectively)[29] and comparable to reported Sn(II)−Cl bond lengths.[23,30−34] The tin-cryptand complex has tin−oxygen and tin−nitrogen distances averaging 2.84 and 2.85 Å, respectively. The Sn−N bonds are longer than reported covalent Sn(II)−N bond lengths[30,34−36] and the Sn−O (cryptand) distances are longer than reported covalent Sn(II)−O bond lengths,[30,34−37] but comparable to those in the related tin(II)-crown ether complexes (**5**−**9**).[23−25,38]

The X-ray data of **11** (Supporting Information, Figure S2) reveal similar metrics to **10**. Selected bond lengths are listed in Table 1. The tribromidostannate anion has bond distances of 2.6238(11), 2.6058(11), and 2.6178(10) Å, consistent with literature values.[39] The long tin−tin distance of 7.139(1) Å and an average of 7.553(2) Å between the anionic bromide and the cationic tin is evidence that there is no interaction between the anion and the cation. The cationic moiety contains a Sn(II)−Br bond of 2.6879(11) Å, consistent with literature values.[40−42] Distances between the tin and the heteroatoms of the cryptand are similar to those in **10**. No suitable crystals for X-ray diffraction were obtained for **12**.

To assess the extent of interaction between the heteroatoms of the cryptand and the tin centers and to better understand the electronic structures of these systems, Natural Bond Order (NBO) analyses and Natural Population Analyses (NPA)[43] were carried out on all complexes.

As was observed in **1**,[15] the Wiberg bond indices (WBI) between the tin and the cryptand oxygen atoms range from 0.06 to 0.13, below the value of 1.0 expected for a single covalent bond. The corresponding values for nitrogen and tin range from 0.09 to 0.13 and also suggest no significant interaction. In contrast, there is a stronger bonding interaction with the halogen in **10**−**12**. The Sn−Cl bond is the weakest with a Wiberg bond index of only 0.54. While this is not as large as would be expected for a nonpolar single bond, it is clearly more significant compared to the WBI between the tin and the heteroatoms of the cryptand. The WBI of the Sn−Br bond is 0.61 while the interaction with I is 0.71. The tin-iodide bond exhibits the highest bond order presumably because of the superior orbital overlap between the similarly sized tin and iodine atoms and/or the more compatible hard−soft interactions. From the NPA data for these complexes, the positive charge remains centered on tin. The monocationic halide complexes (**10**−**12**) feature charges on tin ranging from +1.10 to +1.26. The lower Sn-X bond orders correspond to a higher residual positive charge on tin.

^{119}Sn Mössbauer effect (ME) spectroscopic studies were carried out on all compounds. ME spectra of all compounds consisted of well-resolved doublets, characteristic for ^{119}Sn and isomer shifts (ISs) consistent with tin in the +2 oxidation state. The hyperfine parameters of each complex at 90 K are summarized in Table 2.

The ME spectra of **10** were examined over the temperature range 90 < T < 216 K and consisted of an asymmetric broad line resonance in addition to a resonance due to a small impurity of SnO_2 at an IS close to zero. The signal assigned to SnO_2 accounts for about 3% of the total area at 90 K (Figure 2). The major resonance is readily decomposed into two doublets, one corresponding to the anion $SnCl_3^-$, assigned by comparison to literature values,[21,22] and the other to the cation **10**$^+$. The signal assigned to **10**$^+$ exhibits a considerably smaller quadrupolar splitting (QS) than was seen in **5**^{25b} along with a larger IS suggesting higher symmetry at the Sn atom related to greater s character in the lone pair. These findings are also consistent with a higher NBO charge in **5**^{25b} (+1.47) compared to **10** (+1.10), albeit using a different functional. From Figure 2, the areas of the two sites are not equal, and indeed the area ratio is strongly temperature dependent. At 90 K, the area ratio (cation site/anion site) is approximately 1.7. Because of the temperature dependence of the recoil-free fraction, f, which for an optically thin absorber scales directly with the temperature-dependence of the spectral area ($A(T)$) under the resonance curve, the area is different for the two tin sites vide infra. A comparison of the temperature-dependencies is summarized graphically in Figure 3. As expected, the area ratio extrapolates

dx.doi.org/10.1021/ic3006713 | Inorg. Chem. 2012, 51, 7306−7316

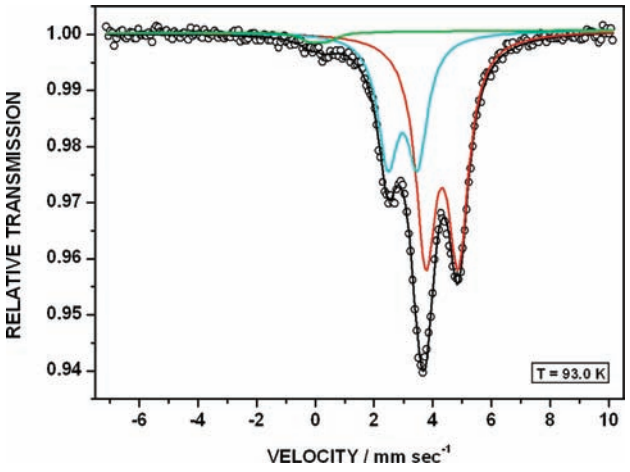

Figure 2. ^{119}Sn Mössbauer spectrum of **10** at 93.0 K. The cation resonance (red) and anion resonance (light blue) components are indicated. The presence of a small amount of SnO_2 is shown by the green curve.

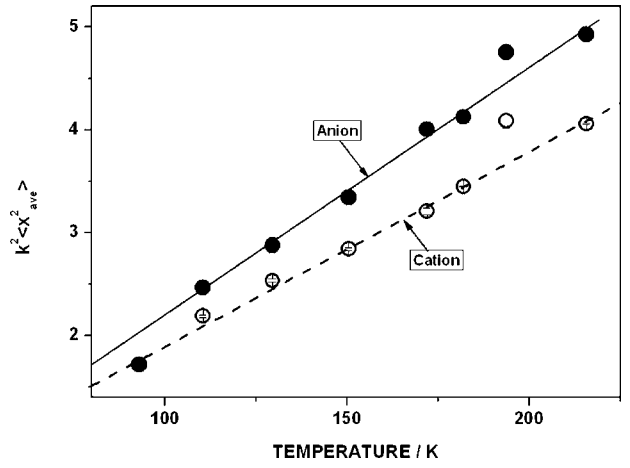

Figure 3. $k^2\langle x^2_{ave}\rangle$ versus temperature for the two Sn sites in **10**. The filled points reflect the anion data, and the open points the cation data.

to ~1 at the low temperature limit in which the respective recoil-free fractions are assumed to approach unity (ignoring the zero-point motion in each case).

The temperature dependencies of the recoil-free fractions are well fit by a linear regression and amount to $(-18.9 \pm 0.2) \times 10^{-3}$ and $(-26.3 \pm 1.3) \times 10^{-3}$ K^{-1} for the cation and anion, respectively. In both cases the correlation coefficients (**R**) are better than 0.99 for 8 data points. As reported earlier,[44] this temperature dependence can be used to evaluate the mean-square-amplitude-of-vibration (msav) of the metal atom and permits comparison of these values with those extracted from single crystal X-ray data (U_{ij} values), and are most conveniently expressed as $\mathcal{F} = k^2\langle x_{ave}{}^2\rangle$, where k is the wave vector of the ME gamma ray ($k^2 = 1.464 \times 10^{18}$ cm^2). For the anion, the two values are $\mathcal{F}_{X,150}$ =3.84 ± 0.04 and $\mathcal{F}_{M,150}$ = 3.87 ± 0.04 respectively, where the X and M subscripts refer to the X-ray and ME data, respectively. For the cation, the two values are $\mathcal{F}_{X,150}$ = 4.86 ± 0.04 and $\mathcal{F}_{M,150}$ = 2.83 ± 0.04. An obvious question now arises, why is the agreement between the X and M data so satisfactory in the case of the anion, but not at all in the case of the cation. As has been discussed earlier,[45] the X-ray data (time scale 10^{-14} s) reflect not only the metal atom vibrations per se but are also sensitive to static lattice imperfections as well as low frequency librational and/or vibrational modes (time scale 10^{-4} to 10^{-5} s), whereas the Mössbauer data (time scale 10^{-8} s) are not sensitive to these low frequency modes; at most the absorption lines are slightly broadened, but the original spectral area is the same.[46−49] The differences between the msav values determined by X-ray and ME methodologies has been extensively discussed for the case of iron in biomolecules by Parak and co-workers.[46,47,50] In the case of the anion, the low frequency modes are absent, whereas in the cation, the cryptand-Sn-Cl bonding geometry is sensitive to the librational modes referred to above because of the absence of strong covalent bonds.

The ME spectra of **11** (Supporting Information, Figure S3) are very similar to those observed for **10**, which was expected. The small difference between **10** and **11** can be accounted for by the substitution of Cl by Br. The temperature dependencies of the derivative of the logarithm of the spectral area, −d ln $[A(T)/A(90)]$/dT (Supporting Information, Figure S4), are included in Table 2 and, again, show that the metal atom in the cation site is more strongly ligated than that in the anion site. These temperature dependencies are, again, well-fit by a linear regression and yield the $\mathcal{F}$ values of 2.54 ± 0.14 and 3.01 ± 0.09 for the ME and X-ray data for the cation and 3.59 ± 0.14 and 4.16 ± 0.08 for the anion, respectively, at 150 K. Here, the comparison between the ME derived value and the X-ray derived value are not in good agreement for reasons that are not obvious from the presently available data. Indeed, it was expected that the agreement for the $SnBr_3^-$ anion would be comparable to the chloride homologue, above, but this is not the case. The cation, similar to **10**$^+$, is more susceptible to the librational modes, which can account for the poor agreement between the ME and X-ray values.

The ME spectra of **12** were obtained, but because of the nonresonant scattering of the heavy I atoms, the effect magnitude observed at all temperatures was very small. This sample contained a large amount of a SnO_2 impurity making extraction of the hyperfine parameters difficult and unreliable.

Table 3. Spectral ^{119}Sn SSNMR Parameters of 10−13 and Various Stannates

complex	δ_{iso} (ppm) anion	Ω (ppm) anion	κ anion	δ_{iso} (ppm) cation	Ω (ppm) cation	κ cation
10	5(1)	880(100)	1	−980(1)	1060(100)	0.75(10)
11	165(1)	890(100)	0.95(5)	−920(1)	1180(100)	0.7(1)
12	50(50)	700(100)	0.75(10)	−810(50)	1400(200)	0.8(1)
13				−1533(1)	165(10)	0.2(1)
$[NBu_4][SnCl_3]$	2(5)	805(50)	1			
$[NBu_4][SnBr_3]$	125(1)	790(100)	0.8(1)			
$[NBu_4][SnI_3]$	250(50)	900(100)	0.8(1)			
$[NBu_4][SnClI_2]$	130(50)	1000(100)	0.45(10)			

dx.doi.org/10.1021/ic3006713 | Inorg. Chem. 2012, 51, 7306−7316

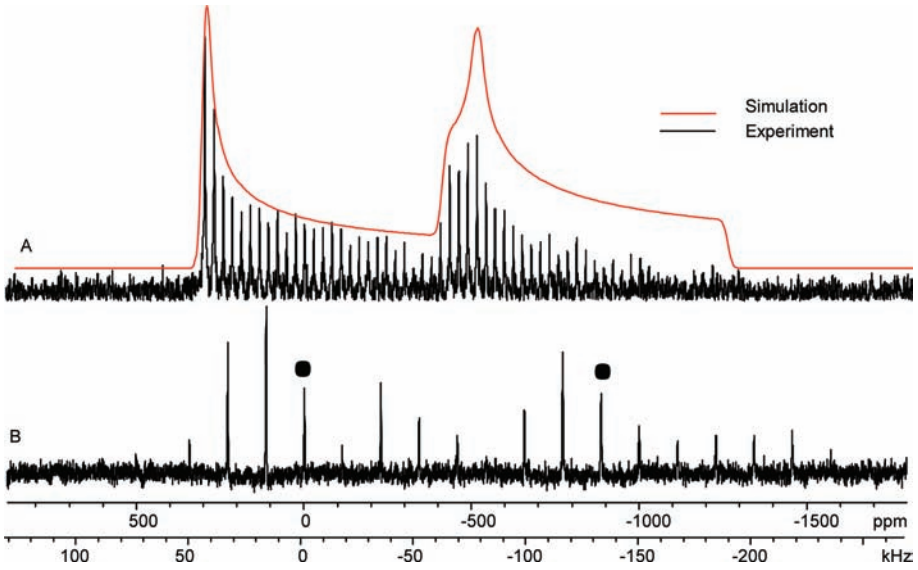

Figure 4. (A) Static ^{119}Sn WURST-CPMG spectrum of **10**. The solid red trace indicates the simulated spectrum. (B) ^{119}Sn MAS spectrum (ν_{rot} = 17 kHz) of **10**. The solid dots indicate the isotropic shifts of the signals.

^{119}Sn NMR spectroscopy was also used to characterize the complexes **10**−**12**. ^{119}Sn possesses a large chemical shift range from 4000 to −2500 ppm, and thus, the isotropic shift is extremely sensitive to structural changes. The use of solid-state NMR spectroscopy allows insight into the bonding of a tin complex through the examination of the tensors. In a nonspherically symmetric environment, tin exhibits large chemical shielding anisotropies (CSA) in the solid-state. In solution, the CSA based relaxation often leads to considerable broadening at moderate (B_0 > 5.97 T) magnetic fields.

Unfortunately, no signals were observed in the solution-state for complexes **10**−**12**; however, ^{119}Sn solid-state NMR data were collected using both magic angle spinning (MAS) and static conditions. Isotropic shifts were determined by acquiring MAS spectra at two different spinning speeds, except in the case of the iodine containing compounds which were determined by spectral simulation. The parameters are summarized in Table 3. The overall tin concentration in these complexes is low because of the large size of the encapsulating cryptand, leading to noisy spectra even after long acquisition times.

The MAS spectrum of **10** (Figure 4B) is composed of two signals with isotropic shifts of 5 ppm and −980 ppm. An isotropic shift of 5 ppm is consistent with solution state data for the $SnCl_3^-$ anion.[51] The isotropic shift differs from that reported for **5**;[25b] however, the experiment was performed at a much lower spinning speed (11 kHz versus 17 kHz), leading to the possibility of temperature effects. The assignment was confirmed by preparing the anion independently as the $[NBu_4][SnCl_3]$ salt.[28] The ^{119}Sn SSNMR spectrum of the ammonium salt closely resembles the less shielded signal of the complex (Supporting Information, Figure S5). The more shielded signal must, therefore, arise from the cationic portion of **10**. While not consistent with the expected chemical shift of a stannylium ion,[52] the chemical shift of the tin(II) cationic crown ether/glyme complexes were also considerably shielded[25] which has been attributed to the high s character of the tin lone pair leading to a relatively small paramagnetic shielding term.[53] The more negative isotropic shift value for the cation in **10** compared to that in **5** suggests that there may be greater s character in the lone pair of **10**, consistent with the NBO and the ME results.

Because of the large CSA pattern, the WURST-CPMG pulse sequence was employed, which is based on the Carr−Purcell−Meiboom−Gill pulse sequence; however, rather than hard $\pi/2$ and π pulses, adiabatic WURST (Wideband Uniform Rate Smooth Truncation) pulses are used for both excitation and refocusing purposes. By using these shaped pulses, it is possible to excite a larger region than would be possible with a hard pulse. Additionally, the use of refocusing pulses enhances the signal-to-noise ratio of the spectrum.

From the static spectrum of **10** (Figure 4A), it is apparent that the anionic signal arises from an axially symmetric environment (κ = 1), consistent with the C_3 axis through the trichloridostannate anion as observed crystallographically. The skew value of the cationic signal (0.75) is consistent with the absence of specific site symmetry about tin in the structure. Both signals exhibit considerable chemical shielding anisotropy (Ω = 880 ppm and 1060 ppm, respectively) consistent with the absence of spherical symmetry about both tin atoms in the complex differing from what was observed in the crown ether complexes, **7**−**9**.[24] In those complexes, there was a small span and a near zero skew because of the high symmetry at tin. In the case of **10**, the attached chloride disrupts both spherical and axial symmetry leading to a greater orientation dependence. Combined with the larger IS and smaller quadrupolar splitting in the Mössbauer spectrum, the smaller span in **10**, when compared to **5**,[25b] suggests that the lone pair has lower p character.

While the MAS spectrum of **11** (Supporting Information, Figure S6B) exhibits a considerably poorer signal-to-noise ratio attributed to the observed shorter T_2 relaxation as well as the lower overall tin concentration in the same sample volume as compared to **10**, it bears an overall resemblance to that of **10**. The spectrum once again consists of two broad signals. The less shielded signal, with an isotropic shift of 165 ppm, is assigned to the tribromidostannate anion.[51] In this case, the anion site falls slightly short of perfect axial symmetry (κ = 0.95), consistent with slight deviations from C_{3v} symmetry observed in the structure of this anion.[28] The isotropic shift of the more

dx.doi.org/10.1021/ic3006713 | Inorg. Chem. 2012, 51, 7306−7316

shielded signal is similar to that of **10** (δ_{iso} −920) and exhibits no specific symmetry (κ = 0.7). The nature of the anionic site was once again confirmed by comparison to the ^{119}Sn SSNMR spectrum of the tetrabutylammonium salt (Supporting Information, Figure S7). While the isotropic shift of $[NBu_4][SnBr_3]$ (δ_{iso} 125) differed from that seen in the complex, the overall line shape was the same within experimental error. The difference in isotropic shift suggests some degree of interaction between the cation and anion in complex **11**.

The static WURST-CPMG spectrum of **11** (Supporting Information, Figure S6A) at first glance appears to consist of only one signal. However, a second, considerably weaker signal is present in the region expected for the signal derived from the anion in **11**. Likely, the anion in **11** relaxes more rapidly than the cation because of the three covalently bound bromine atoms. With a much shorter T_2, the signal receives considerably less signal enhancement than the cation. The major signal in the WURST-CPMG spectrum of **11**, as expected from the MAS spectrum of **11**, very closely resembles the cationic portion of **10**. As the ^{119}Sn SSNMR spectra of the two known complexes very closely resembled each other, it was hoped that ^{119}Sn SSNMR spectroscopy would also offer an insight into the unknown structure of **12**.

Attempts to obtain an MAS spectrum of **12** were ultimately unsuccessful. However, it was possible to acquire a static WURST-CPMG spectrum (Supporting Information, Figure S8). The signal at δ_{iso} −810 exhibited a similar line shape (Ω = 1400 ppm, κ = 0.8) to the cationic sites in the ^{119}Sn SSNMR spectra of **10** and **11**. The isotropic shift of the signal is not as shielded as those of **10** and **11**, indicating the highest occupied molecular orbital (HOMO) has greater p character. Because of the absence of a MAS spectrum, the standard uncertainties in the parameters of **12** are much greater, but the overall line shape is undeniably similar to the cationic signals of **10** and **11**. Similar to **11**, the signal attributed to the anion (δ_{iso} 50) is less intense than that of the cation. The signal has the expected line shape (Ω = 700 ppm, κ = 0.75) for a system distorted from axial symmetry. The triodidostannate anion was prepared independently as the $[NBu_4][SnI_3]$ salt.[28] The ^{119}Sn static WURST-CPMG spectrum of the salt (Supporting Information, Figure S9) resembled the deshielded signal of **12**, although the isotropic shift was considerably less shielded (δ_{iso} 250, Ω = 900 ppm, κ = 0.8).

An attempt was made to prepare **12** by the addition of trimethylsilyl iodide to a solution of $SnCl_2$ and cryptand[2.2.2], rather than by the addition of cryptand[2.2.2] to SnI_2. A yellowish solid was obtained (**12′**) that had virtually identical ^{1}H NMR and Raman data to those of **12** but significantly different ^{119}Sn SSNMR and ESI-MS spectra. The ^{119}Sn SSNMR WURST-CPMG spectrum of the solid contained two apparent signals (Supporting Information, Figure S10). While the line shape of the upfield signal at δ_{iso} −945 resembles that of the analogous signal in the ^{119}Sn SSNMR spectrum of **12**, the apparent isotropic shift is more shielded, closer to the values observed for the cations in **10** and **11**. The downfield signal differed considerably from the analogous signal assigned to the anion of **12**. While the isotropic shift of the downfield signal initially appeared reasonable (δ_{iso} 0(50)), the overall line shape (Ω = 880 ppm, κ = −0.3(2)) was not consistent with the near axially symmetric geometry expected for the triodidostannate anion,[28] leading to the conclusion that the anion in this solid cannot be SnI_3^-. A signal, assigned to the $SnClI_2^-$, was observed in the ESI negative mode mass spectrum of **12′**, and thus, the tetrabutylammonium salt of $SnClI_2^-$ was prepared and its ^{119}Sn SSNMR WURST-CPMG spectrum recorded (Supporting Information, Figure S11). As expected from the lower symmetry, the skew value does not correspond to any specific site symmetry (κ = 0.45). The experimental ^{119}Sn SSNMR spectrum of **12′** (Supporting Information, Figure S10) was reproduced using a combination of the parameters for both the cation of **10** and **12** and a combination of the parameters for the SnI_3^- and $SnClI_2^-$ anions plus the parameters for a small amount of SnO_2. We conclude that the attempted preparation of **12** via halogen exchange was not successful. The halide exchange in both the cation and the anion apparently did not go to completion, and thus, the preparation of **12** from SnI_2 is the preferred method.

Density functional theory (DFT) calculations of the ^{119}Sn NMR shieldings of **10**−**12** were performed using the Amsterdam Density Functional (ADF)[54] software package using the VWN-BP functional. The all electron quadruple-ζ basis set plus polarization (Q4ZP) was employed for tin, while the triple-ζ doubly polarized (T2ZP) basis set was used for all other atoms. The Zeroth Order Regular Approximation (ZORA) was employed to account for relativistic effects, including the spin orbit term. This methodology was selected as it provided good agreement with the experimental NMR parameters of **7**−**9**.[25] Geometry optimizations of unknown structures were carried out in Gaussian 09[55] using the TPSSTPSS functional and the LANL2DZ basis set on all atoms. Shielding values were converted to chemical shifts relative to the calculated shielding of $SnMe_4$.

In general, the parameters of the anionic sites were more closely reproduced by theory than the cationic sites in complexes **10**−**12**. In the case of the trichloridostannate of **10**, the skew value was exactly reproduced, with both theory and experiment giving an exactly axially symmetric value of 1. The cationic site of **10** was predicted to be much closer to axial symmetry with a skew value of 0.9 versus the 0.75 determined experimentally. The calculated span for $SnCl_3^-$, 855 ppm, is within experimental error of the experimental value of 880 ppm. The span of the cationic signal, $\mathbf{10}^+$, is overestimated (Ω = 1535 ppm vs 1060 ppm) considerably. A similar situation is observed in the case of **11**. The parameters for the anion (Ω = 890(100), κ = 0.95(5)) are reproduced (Ω = 806, κ = 0.89) within experimental error. Once again the cationic site of **11** is not quite as closely reproduced, with an overestimated span (Ω = 1801 ppm vs 1180 ppm) and a more axial symmetry (κ = 0.89 vs 0.7).

Calculations for the iodide complex, **12**, were carried out using a geometry-optimized structure. The predicted skew for the signal assigned to $[SnI_3]^-$ (κ = 0.94) was much closer to what would be expected for an anion with axially symmetric geometry (κ = 1) than the experimentally observed value for the $[NBu_4][SnI_3]$ salt (κ = 0.8), most likely because the gas-phase optimization of the anion produces a more symmetrical structure than what exists in the solid-state. The overestimated span can, similarly, be attributed to the difficulties in reproducing the experimental parameters exactly without an X-ray structure. Of the theoretical parameters for the cationic site of the iodide complex (Ω = 1377 ppm, κ = 0.58), the span is within experimental error (Ω = 1400(200) ppm, κ = 0.8(1)), confirming that the structure of the cationic site is very similar to that of the chloride and bromide derivatives. Geometry optimization of the complex containing the $SnClI_2^-$ anion rather than the SnI_3^- anion gives rise to almost no difference in

dx.doi.org/10.1021/ic3006713 | Inorg. Chem. 2012, 51, 7306−7316

the NMR parameters calculated for the cation. The parameters of the anion (Ω = 845 ppm, κ = 0.38) are in reasonable agreement with those observed for the $[NBu_4][SnClI_2]$ salt, with the skew falling within experimental error and the span being within 1.5 times the experimental error.

On the basis of the extensive data collected, complexes **10**–**12** are monocationic complexes, where the halogen atom is covalently bound to the tin atom. Each complex contains a homoleptic stannate anion. For compounds **10** and **11**, the long distances between the central tin cation and the heteroatoms of the cryptand as determined by X-ray diffraction analysis and NBO calculations indicate no significant bonding between the two species. Although the X-ray structure of **12** was not obtained, we believe, on the basis of the solid-state NMR and ESI-MS data, that the structure of the cation is analogous to the structure of the cations of **10** and **11**. Complex **12** is best synthesized by the direct addition of cryptand[2.2.2] to SnI_2; the addition of trimethylsilyl iodide to a mixture of $SnCl_2$ and the cryptand does not appear to result in complete halogen exchange. ^{119}Sn NMR spectroscopic data of the solid prepared in this way are more consistent with a mixture of $[cryptand[2.2.2]SnCl]^+$ and $[cryptand[2.2.2]SnI]^+$ as the cations and a mixture of SnI_3^- and $SnClI_2^-$ anions.

2.2. Triflate Complex. Trifluoromethanesulfonate (OTf) is a weakly coordinating anion.[56] Trimethylsilyl trifluoromethanesulfonate was added to a solution of $SnCl_2$ and cryptand[2.2.2] in an attempt to abstract the halide. An alternate synthetic route was also explored: cryptand[2.2.2] was added to a solution of tin(II) trifluoromethanesulfonate in THF. Both methods resulted in the formation of the same compound, **13** (Scheme 1).

The solution state ^{19}F NMR spectrum of **13** contained a single signal at δ −79.36, the chemical shift of which is consistent with an ionic triflate as determined by comparison of the chemical shift of **13** with the chemical shifts of MeOTf as a prototypical covalently bonded organic triflate (δ −75.4)[57] and $[Bu_4N][OTf]$ as a prototypical ionic triflate (δ −78.7).[58] The FT-Raman spectrum of **13** revealed the appropriate stretches and deformations correlating to a triflate anion.[59]

The ESI-MS spectrum of **13** (Supporting Information, Figure S12) revealed a mass cluster centered at m/z 645 corresponding to $^{12}C_{19}{}^{1}H_{36}{}^{14}N_2{}^{16}O_9{}^{120}Sn{}^{19}F_3{}^{32}S$; consistent with the presence of a cryptand, a tin and a triflate moiety. Interestingly, a cluster centered at m/z 248 was also observed, which is consistent with a dicationic tin-cryptand complex. Accordingly, the mass cluster at m/z 248 is centered at 1/2 the calculated molecular weight, and the distance between each peak within the cluster is 0.5 m/z units.

X-ray quality crystals of **13** were grown from a concentrated solution of THF, and data were collected at low temperature (Figure 5). The data reveal two crystallographic tin sites, Sn(1) and Sn(2), both associated with cryptand ligands, and four triflate moieties within a formula unit, one of which is disordered. Selected bond lengths are listed in Table 1. As noted in the halogen derivatives **10** and **11**, the tin-cryptand oxygen and nitrogen bonds are all elongated in comparison to covalent Sn(II)–O/N bonds, but are within the range reported for crown ether complexes, **5**–**9**.[23–25,38] Three triflate anions are completely separated from the tin center given the long tin-triflate oxygen distances which range from 2.698(4) to 6.094(4) Å and the S–O bonds all being approximately of equal length. Although an oxygen (O(22)) of the disordered triflate is in close proximity to one of the tin atoms (Sn(2)) in one site

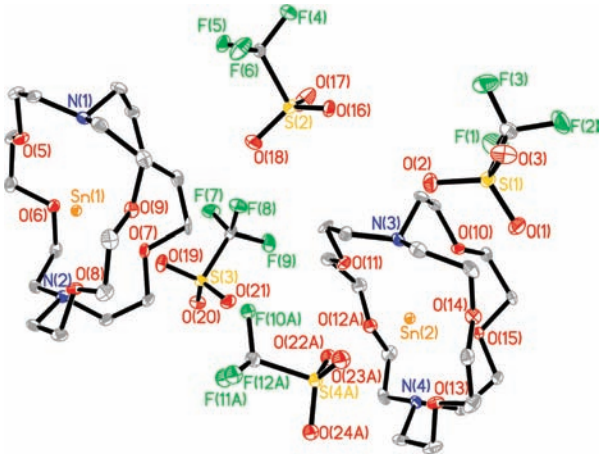

Figure 5. Thermal ellipsoid plot (30% probability surface) of **13**. Selected bond lengths are given in Table 1.

suggesting the possibility of a weak bonding interaction, the quality of the data does not permit a definite conclusion.

NBO calculations also offer the opportunity to quantify the nature of the interactions between the two crystallographically distinct tin atoms and the cryptand moieties. Calculations were performed for Sn(1) and Sn(2) separately. The Wiberg bond index of the Sn(2)–O(22) (triflate) interaction is only 0.14, which is not significantly greater than the bond index between the tin center and the cryptand oxygens, which range from 0.10 to 0.13. The value of 0.14 is also not significantly greater than the value between the Sn(1) center and the nearest triflate oxygen (0.10), suggesting that there is no significant bonding present. While the calculated bond orders of the two tin atoms did not differ significantly, the calculated residual positive charge on each tin center gave significantly different results. The Sn(2) atom has a calculated charge of +1.25. While this is greater than the expected +1 charge for a generic monocation, it is very similar to the value calculated for **10** (+1.26). The Sn(1) atom, in contrast, has a calculated charge of +1.44, very similar to the +1.38 calculated for **1**,[15] although not as large as the NBO charges reported for the crown ether/glyme complexes of $Sn(OTf)_2$ (+1.64).[25b]

The ^{119}Sn Mössbauer spectrum (Supporting Information, Figure S13) of **13** consists of a single (major) Sn resonance with a small quadrupole interaction, as well as an impurity at an IS close to zero, which can be assigned to SnO_2.[60] The IS of **13** (4.40 mm sec^{-1}) is the largest of all the complexes, indicating that there is more s-electron character consistent with a more ionic tin center. The small quadrupolar splitting of **13** (0.6 mm sec^{-1}) is indicative of a more symmetrical environment compared to **10** and **11**, and consistent with the tin atom only weakly associating with the heteroatoms of the cryptand and one triflate anion. The ME parameters of **13** are comparable to those of the crown ether complexes of **7**–**9**.[25b] The IS and QS parameters of the major resonance are only moderately temperature dependent and do not justify extraction of M_{eff} and Θ_M values from the available data. On the other hand, the temperature-dependence of f is well accounted for by a linear regression (**R** = 0.99 for 7 data points), and thus, yields a value of $\mathcal{F}_{M,150}$ = 2.630 ± 0.027 from the ME data and $\mathcal{F}_{X,150}$ = 2.631 ± 0.085 from the X-ray data, in excellent agreement with each other.

The ^{119}Sn SSNMR static spectrum (Figure 6A) of **13** differed considerably from the analogous spectra of the halide

dx.doi.org/10.1021/ic3006713 | Inorg. Chem. 2012, 51, 7306–7316

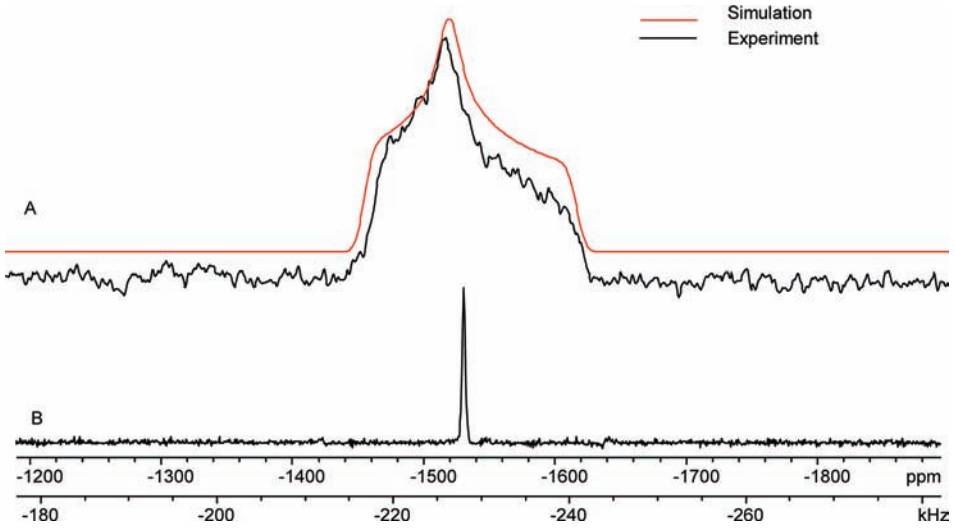

Figure 6. (A) Static ^{119}Sn spin echo spectrum of **13**. The solid red trace indicates the simulated spectrum. (B) ^{119}Sn MAS spectrum ($\nu_{ro}t$ = 16 kHz) of **13**.

complexes, **10**−**12**. The signal was considerably narrower, and therefore, the spectrum was acquired using a static echo sequence. The much narrower spectrum, with κ = 0.2 and Ω = 165 ppm, is consistent with what was observed for the tin crown ether complexes (**7**−**9**) and most similar to the Sn[15-crown-5]$^{2+}$ complex **8**.[25] The somewhat higher skew value is likely due to the distortion of the cryptand observed crystallographically. Additionally, the isotropic shift of **13** (δ_{iso} −1533) is consistent with the dicationic complexes **7**−**9** (**7** (δ_{iso} −1405), **8** (δ_{iso} −1721 and −1706)), albeit the shift of **13** is most similar to the isotropic shift of the monocationic complex **9** (δ_{iso} −1578). In contradiction to what was expected from the crystal structure, only one ^{119}Sn signal was observed under MAS conditions (Figure 6B). This is further supported by the solid-state ^{19}F NMR spectrum of **13** (Supporting Information, Figure S14), which features two fluorine resonances rather than the four expected on the basis of the crystal structure. Both fluorine resonances possess isotropic shifts (δ_{iso} −78.3 ppm and −80.5 ppm) consistent with ionic triflates.[57]

Theoretical parameters for both crystallographically distinct tin atoms, Sn(1) and Sn(2), from the X-ray structure were determined using the same computational techniques as the halide derivatives. While neither set of parameters exactly matched experiment (δ_{iso} −1533, Ω = 165 ppm, κ = 0.2), the calculated parameters for Sn(1) (δ_{iso} −1520, Ω = 275 ppm, κ = −0.05) more closely resembled the experimental data for **13** than the calculated parameters for Sn(2) (δ_{iso} −1165 ppm, Ω = 531 ppm, κ = 0.11). The theoretical parameters for Sn(2) more closely resemble those observed experimentally for **10**−**12**, with a more deshielded isotropic shift and a larger span. The theoretical parameters further support the MAS data which suggests that there is only one tin complex present in the bulk sample.

Isotropic shifts were systematically overestimated for all compounds, **10**−**13**, suggesting that the difficulty may partially lie with the calculated value for the shielding of the standard. There is a linear (R^2 = 0.96) correlation between the experimental and calculated shifts (Supporting Information, Figure S15). If there were perfect 1:1 agreement between the experimental and theoretical isotropic shifts, the slope of the line in Supporting Information, Figure S15 would be exactly 1; however, the slope is 1.25, suggesting that while there is a systematic overestimation, the overall agreement between the experimental and theoretical shifts remains reasonable. While the span and skew of the signals attributed to the anions were generally better reproduced compared to those of the cations, the opposite appears to be true for the isotropic shift. The theoretical shifts of the cations lie much closer to the 1:1 line than those of the anions.

From the available data for **13**, we believe that a tin atom is within the cavity of cryptand[2.2.2] forming a dicationic complex. Although the monocationic species was observed in the ESI-MS spectrum, this may be accounted for by aggregation in the gas phase. Notably, a signal assigned to the monocation of the germanium(II) cryptand complex was also observed in the mass spectrum of the dication **1**.[15] The single tin signals in the both ^{119}Sn ME and SSNMR spectra support the assignment of the dicationic complex. The chemical shift of the single signal in the ^{19}F NMR spectrum in solution of **13** and the two signals in the solid-state spectrum are also both indicative of an ionic triflate.

3. SUMMARY

To conclude, the reaction between a tin(II) precursor and cryptand[2.2.2] results in the formation of either a tin(II) monocationic complex with the cryptand where a halogen atom is covalently bonded to the tin atom or a dicationic tin(II) cryptand complex with triflate as the counterion. The results are in contrast with the analogous germanium chemistry, which produced a dicationic Ge(II) complex with cryptand[2.2.2] (**1**) with a halide precursor.[15] This difference could simply be attributed to the size of tin versus germanium, with the larger tin favoring a higher coordination number. The larger tin cation may require a larger cryptand to encapsulate it completely. However, the diameter of the cavity in cryptand[2.2.2], in its optimal conformation, is 2.80 Å,[18] seemingly sufficient to encapsulate tin(II) which has an ionic radius of 1.12 Å.[29] Lead(II), with an ionic radius of 1.19 Å,[29] complexes with cryptand[2.2.2] to give either a mono- or dicationic complex with external coordination with water or the counterions.[18,19] The behavior of tin(II) falls between that of germanium(II) and lead(II); depending on the available ligands, the tin maintains a

dx.doi.org/10.1021/ic3006713 | Inorg. Chem. 2012, 51, 7306−7316

Table 4. Crystallographic Data for Complexes 10, 11, and 13

	10	11	13
empirical formula	$C_{18}H_{36}C_{l4}N_2O_6Sn_2$	$C_{18}H_{36}Br_4N_2O_6Sn_2$	$C_{40}H_{72}F_{12}N_4O_{24}S_4Sn_2$
formula weight	755.67	933.51	1585.63
crystal system	monoclinic	monoclinic	monoclinic
space group	$P2(1)$	$P2(1)$	$P2(1)/c$
a (Å)	8.4411(11)	8.4816(17)	12.7912(12)
b (Å)	11.2137(15)	11.541(2)	30.622(3)
c (Å)	14.493(2)	14.656(3)	18.8561(14)
α (deg)	90.00	90.00	90
β (deg)	91.529(9)	90.21(3)	125.400(5)
γ (deg)	90.00	90.00	90
volume (Å^3)	1371.4(3)	1434.6(5)	6020.4(9)
Z	2	2	4
data/restraints/parameters	6406/1/290	6366/1/290	12313/9/796
goodness-of-fit	0.953	1.105	1.001
R [$I > 2\sigma(I)$]	0.0550	0.0373	0.0447
wR^2 (all data)	0.1318	0.1129	0.0940
largest diff. peak and hole (e Å^{-3})	1.661, −1.516	1.228, −1.659	0.799, −0.775

covalent bond and forms a monocationic complex, or interacts solely with the heteroatoms of the cryptand and forms a dicationic complex.

An interesting comparison is made between the SnCl macrocyclic polyether complexes **5** and **10** where the crown ether has been replaced by the cryptand. Both the ME and ^{119}Sn NMR data suggest that there is greater s electron density at Sn and the electron density is more spherically symmetric in **10** compared to **5**. A comparison of the spectral data of the Sn-triflate macrocyclic polyether complex **13** to the analogous crown ether complexes suggests the electronic structures are very similar with both types of complexes having quite spherically symmetric electron density in an orbital of high s character about the Sn. With a clear understanding of the structure and bonding in these highly interesting complexes, we will now undertake an investigation of their reactivity.

4. EXPERIMENTAL SECTION

All manipulations were carried out under an anhydrous N_2 atmosphere using standard Schlenk line and glovebox techniques at room temperature. Tetrahydrofuran (THF), hexanes, and acetonitrile were dried by passing through an alumina column and then stored over 4 Å molecular sieves. CD_3CN was distilled over CaH_2 and then stored over 4 Å molecular sieves. NMR chemical shifts are reported in ppm. The ^{1}H NMR spectra were referenced internally to the residual CD_2HCN resonance at 1.94 ppm. The ^{19}F NMR spectra were referenced externally to $CFCl_3$ (0 ppm) or to C_6H_5F (−113.1 ppm relative to $CFCl_3$). All other chemicals were purchased from commercial sources and used without further purification. FT-Raman spectra of the bulk material are reported in cm^{-1} and were collected under a N_2 atmosphere in a sealed melting point tube. Elemental analyses of the new compounds were not obtained because of their air and moisture sensitivity.

X-ray Crystallography Experimental Details. Each crystal was covered in Nujol and placed rapidly into the cold N_2 stream of a Kryo-Flex low temperature device. The data were collected either by employing the SMART[61] software on a Bruker APEX CCD diffractometer or by using the COLLECT[62] software on a Nonius KAPPA CCD diffractometer, each being equipped with a graphite monochromator with Mo Kα radiation (λ = 0.71073 Å). For each sample, a hemisphere of data was collected using counting times of 10−30 s per frame. The data were collected at −123 °C. Data reductions were performed using the SAINT[63] software, and the data were corrected for absorption using SADABS[64] or using the DENZO-Scalepack application.[65] The structures were solved by direct methods using the SHELX[66] suite of programs and refined by full-matrix least-squares on F^2 with anisotropic displacement parameters for the non-H atoms using SHELXL-97[66] and the WinGX[67] software package. Details of the final structure solutions were evaluated using PLATON,[68] and thermal ellipsoid plots were produced using SHELXTL.[66] Crystallographic data are listed in Table 4.

^{119}Sn Mössbauer Spectroscopy. Samples of **10**−**13** were shipped from Canada to Israel under strictly anhydrous conditions in O-ring sealed sample holders. These sample holders were then transferred within a few seconds to liquid nitrogen storage prior to mounting cold in the spectrometer cryostat. The samples were examined in transmission geometry as described previously[69] using a $CaSnO_3$ source at room temperature. Spectrometer calibration and temperature monitoring were effected as described previously, and all ISs are reported with reference to a room temperature $BaSnO_3$ absorber spectrum. Data fitting assuming Lorentzian lineshapes, was carried out using a matrix inversion least-squares fitting routine.

^{119}Sn SSNMR Spectroscopy. All solid-state NMR spectra were acquired on a Varian Infinity 400 MHz spectrometer. Experimental setup and pulse width calibration for one pulse and spin echo experiments were performed on solid tetracyclohexyltin. Chemical shift referencing was performed relative to this sample (−97.3 ppm relative to $SnMe_4$). Optimization of the WURST-CPMG[70] sequence was carried out on tin(II) oxide.

MAS experiments were carried out using a 4 mm HXY MAS probe in dual resonance mode. A one pulse sequence with proton decoupling with a pulse width corresponding to a 30 degree pulse was employed; recycle delays were selected to allow full relaxation. Static experiments were carried out using an HX static probe in dual resonance mode. The majority of these experiments employed a WURST-CPMG sequence consisting of a WURST-80 pulse followed by a series of identical refocusing pulses. For the triflate complex, a standard (π/2-τ-π-τ-acquisition) spin echo experiment was employed.

SSNMR Spectral Simulation. Experimental parameters were determined by analytical simulations using WSolids.[71] MAS spectra were analyzed using the Herzfeld−Berger analysis package included with WSolids. Errors were determined by visual comparison to the experimental spectrum. Starting from the best fit value, the parameter being evaluated was varied systematically in both directions while all others were held constant until a visible change was observed.

Theoretical Calculations. Geometry optimizations were performed in Gaussian 09[55] using the TPSSTPSS[72] functional and the LANL2DZ basis set on all atoms. Calculation of ^{119}Sn CS parameters was carried out in ADF[72] using the BPVWN functional and a Q4ZP basis set on tin with T2ZP employed on all other atoms. All electron basis sets were optimized for the ZORA method. All calculations were performed on the Shared Hierarchical Academic Research Computing

dx.doi.org/10.1021/ic3006713 | Inorg. Chem. 2012, 51, 7306−7316

Network (SHARCNET). Calculations were performed on an 8 core Xeon 2.83 GHz CPU with 16 GB memory.

Direct Synthesis of 10, 12, and 13. In a glovebox, tin(II) chloride (0.05 g, 0.27 mmol), tin(II) triflate (0.05 g, 0.13 mmol), or tin(II) iodide (0.05 g, 0.13 mmol) was dissolved in THF (6 mL) in a 100 mL round-bottomed flask. Cryptand[2.2.2] (0.05 g, 0.13 mmol) was added to the reaction mixture to give a clear, colorless solution. A white (or yellow) solid precipitated from the solution within 1 min. The mixture was allowed to stir for 30 min. Hexanes (6 mL) were added to the solution. The supernatant was removed, and the white (or yellow) solid was placed under high vacuum (0.09 g, 90.0%).

10: White solid. mp: 172−176 °C. ^{1}H NMR (CD_3CN): δ 2.78−2.83 (m, 2H), 3.67 (s), 3.65−3.70 (m, together 4H). $^{13}C\{^{1}H\}$ NMR (CD_3CN): δ 37.9, 69.4, 70.5. Raman: cm^{-1} 2959 (m), 2928 (s), 2886 (s), 2840 (m), 1480 (w), 1462 (m), 1452 (m), 1366 (w), 1294 (w), 1271 (m), 1236 (w), 1165 (w), 1131 (w), 1116 (w), 1096 (w), 1059 (w), 860 (m), 748 (m), 293 (s), 260 (s), 136 (s), 111 (s). LRMS (ESI-TOF): [^{120}Sn·^{35}Cl·cryptand^{+}] m/z 531.1. HRMS (ESI-TOF) found (calcd for $C_{18}H_{36}N_2O_6{}^{35}Cl^{116}Sn$): 527.1265 (527.1279).

12: Yellow solid. mp: 178−180 °C. ^{1}H NMR (CD_3CN): δ 2.84−2.94 (m, 2H), 3.68 (s), 3.68−3.74 (m, together 4H). $^{13}C\{^{1}H\}$ NMR (CD_3CN): δ 37.5, 69.2, 70.1. Raman: cm^{-1} 2884 (m), 1472 (w), 1455 (m), 1274 (w), 856 (w), 748 (w), 304 (w), 133 (s), 85 (m). LRMS (ESI-TOF; positive mode): [^{120}Sn·I·cryptand^{+}] m/z 622.9. LRMS (ESI-TOF; negative mode): [$^{119}SnI_3^{-}$] m/z 500.5. HRMS (ESI-TOF) found (calcd for $C_{18}H_{36}N_2O_6I^{120}Sn$): 623.0633 (623.0604).

13: White solid. Decomposition point 260 °C. ^{1}H NMR (CD_3CN): δ 2.81−2.86 (m, 2H), 3.78 (s), 3.76−3.80 (m, total 4H). $^{13}C\{^{1}H\}$ NMR (CD_3CN): δ 37.4, 69.4, 70.0. ^{19}F NMR (CD_3CN): δ −79.36 (s). Raman: cm^{-1} 2931 (s), 2894 (s), 1471 (m), 1279 (m), 1224 (m), 1170 (w), 1032 (s), 859 (m), 754 (s), 573 (m), 348 (m), 313 (s), 120 (m), 85 (m). LRMS (ESI-TOF): [^{120}Sn·OTf·cryptand^{+}] m/z 645.1, [^{120}Sn·cryptand^{2+}] m/z 248.1. HRMS (ESI-TOF) found (calcd for $C_{19}H_{36}N_2O_9S^{116}SnF_3$): 641.1124 (641.1111).

Syntheses of 11 or 13 by Exchange. In the glovebox, tin(II) chloride (2 equiv) was dissolved in THF (6 mL) in a 100 mL round-bottomed flask. Cryptand[2.2.2] (1 equiv) was added followed by Me_3SiX (X = Br, OTf, 4 equiv). The mixture was allowed to stir for 30 min. Hexanes (6 mL) were added to the mixture; a solid precipitated. The supernatant was removed, and the solid was placed under high vacuum.

11: White solid. mp: 174−178 °C. ^{1}H NMR (CD_3CN): δ 2.84 (br s, 2H), 3.67 (s) 3.64−3.74 (br m, together 4H). $^{13}C\{^{1}H\}$ NMR (CD_3CN): δ 37.6, 69.3, 70.3. Raman: cm^{-1} 2961 (w), 2918 (s), 2907 (s), 2893 (s), 2875 (s), 2836 (m), 2804 (w), 1479 (w), 1465 (w), 1453 (m), 1367 (w), 1293 (w), 1270 (w), 1235 (w), 860 (w), 748 (w), 311 (w), 267 (w), 202 (s), 182 (s), 86 (s). LRMS (ESI-TOF) MS: [^{120}Sn·^{79}Br·cryptand^{+}] m/z 575.3.

■ ASSOCIATED CONTENT

Ⓢ Supporting Information

One document containing the Raman spectrum of **12**, thermal ellipsoid plot of **11**, ^{119}Sn Mössbauer spectra and details of **11** and **13**, ^{119}Sn SSNMR spectra and details of **11**, **12**, **12′** and various stannates, ^{19}F SSNMR and ESI-MS spectra of **13** and crystallographic data for the structural analysis of **10**, **11**, and **13** and one file containing the cif for **10**, **11**, and **13**. This material is available free of charge via the Internet at http://pubs.acs.org.

■ AUTHOR INFORMATION

Corresponding Author

*E-mail: herber@vms.huji.ac.il (R.H.H.), yhuang@uwo.ca (Y.H.), kbaines2@uwo.ca (K.M.B.).

Notes

The authors declare no competing financial interest.

■ ACKNOWLEDGMENTS

Computational work was made possible by the facilities of the Shared Hierarchical Academic Research Computing Network (SHARCNET: www.sharcnet.ca) and Compute/Calcul Canada. We thank the Natural Sciences and Engineering Research Council of Canada and the University of Western Ontario for financial support. We thank Dr. G. Popov, Dr. BFT Cooper, Ms. A. Borecki for assistance with the X-ray crystallography, and Prof. R.W. Schurko (Univ. Windsor) for the WURST-CPMG pulse sequence.

■ REFERENCES

(1) Lee, V. Y.; Sekiguchi, A. *Acc. Chem. Res.* **2007**, *40*, 410.
(2) Zharov, I.; Michl, J. In *The Chemistry of Organic Germanium, Tin and Lead Compounds*; Rappoport, Z., Apeloig, Y., Eds.; Wiley & Sons: Chichester, U.K., 2002; Vol. 2, p 633.
(3) Kim, K.-C.; Reed, C. A.; Elliott, D. W.; Mueller, L. J.; Tham, F.; Lin, L.; Lambert, J. B. *Science* **2002**, *297*, 825.
(4) Lambert, J. B.; Lin, L. *J. Org. Chem.* **2001**, *66*, 8537.
(5) Lambert, J. B.; Lin, L.; Keinan, S.; Müller, T. *J. Am. Chem. Soc.* **2003**, *125*, 6022.
(6) Schenk, C.; Drost, C.; Schnepf, A. *Dalton Trans.* **2009**, 773.
(7) Sekiguchi, A.; Fukawa, T.; Lee, V. Y.; Nakamoto, M.; Ichinohe, M. *Angew. Chem., Int. Ed.* **2003**, *42*, 1143.
(8) Rupar, P. A.; Staroverov, V. N.; Ragogna, P. J.; Baines, K. M. *J. Am. Chem. Soc.* **2007**, *129*, 15138.
(9) Jutzi, P.; Dickbreder, R.; Noth, H. *Chem. Ber.* **1989**, *122*, 865.
(10) Jutzi, P.; Kohl, F.; Hofmann, P.; Krüger, C.; Tsay, Y. *Chem. Ber.* **1980**, *113*, 757.
(11) Jutzi, P.; Mix, A.; Rummel, B.; Schoeller, W. W.; Neumann, B.; Stammler, H.-G. *Science* **2004**, *305*, 849.
(12) (a) Driess, M.; Yao, S.; Brym, M.; van Wüllen, C. *Angew. Chem., Int. Ed.* **2006**, *45*, 4349. (b) Driess, M.; Yao, S.; Brym, M.; van Wüllen, C. *Angew. Chem., Int. Ed.* **2006**, *45*, 6730.
(13) Cheng, F.; Dyke, J. M.; Ferrante, F.; Hector, A. L.; Levason, W.; Reid, G.; Webster, M.; Zhang, W. *Dalton Trans.* **2010**, *39*, 847.
(14) (a) Dutton, J. L.; Ragogna, P. J. *Coord. Chem. Rev.* **2011**, *255*, 1414. (b) Levason, W.; Reid, G.; Zhang, W. *Coord. Chem. Rev.* **2011**, *255*, 1319.
(15) Rupar, P. A.; Staroverov, V. N.; Baines, K. M. *Science* **2008**, *322*, 1360.
(16) Rupar, P. A.; Bandyopadhyay, R.; Cooper, B. F. T.; Stinchcombe, M. R.; Ragogna, P. J.; Macdonald, C. L. B.; Baines, K. M. *Angew. Chem., Int. Ed.* **2009**, *48*, 5155.
(17) (a) Cheng, F.; Hector, A. L.; Levason, W.; Reid, G.; Webster, M.; Zhang, W. *Angew. Chem., Int. Ed.* **2009**, *48*, 5152. (b) Hector, A. L.; Levason, W.; Reid, G.; Webster, M.; Zhang, W. *Dalton Trans.* **2011**, *40*, 694.
(18) Chekhlov, A. *J. Struct. Chem.* **2006**, *47*, 352.
(19) Chekhlov, A. *Russ. J. Coord. Chem.* **2006**, *32*, 552.
(20) Leszczyńska, K.; Mix, A.; Berger, R., J. F.; Rummel, B.; Neumann, B.; Stammler, H.-G.; Jutzi, P. *Angew. Chem., Int. Ed.* **2011**, *50*, 6843.
(21) Herber, R. H.; Carrasquillo, G. *Inorg. Chem.* **1981**, *20*, 3693.
(22) Herber, R. H.; Smelkinson, A. E. *Inorg. Chem.* **1978**, *17*, 1023.
(23) Drew, M. G. B.; Nicholson, D. G. *J. Chem. Soc., Dalton Trans.* **1986**, 1543.
(24) Hough, E.; Nicholson, D. G. *J. Chem. Soc., Dalton Trans.* **1989**, 2155.
(25) (a) Bandyopadhyay, R.; Cooper, B. F. T.; Rossini, A. J.; Schurko, R. W.; Macdonald, C. L. B. *J. Organomet. Chem.* **2010**, *695*, 1012. (b) Macdonald, C. L. B.; Bandyopadhyay, R.; Cooper, B. F. T.; Friedl, W. W.; Rossini, A. J.; Schurko, R. W.; Eichhorn, S. H.; Herber, R. H. *J. Am. Chem. Soc.* **2012**, *134*, 4332.
(26) (a) Tagne Kuate, A. C.; Schürmann, M.; Schollmeyer, D.; Hiller, W.; Jurkschat, K. *Chem.—Eur. J.* **2010**, *16*, 8140. (b) Wolff, M.;

Harmening, T.; Pöttgen, R.; Feldmann, C. *Inorg. Chem.* **2009**, *48*, 3153.
(27) Nakamoto, K. *Infrared and Raman Spectra of Inorganic and Coordination Compounds Part A*; John Wiley & Sons Inc.: Hoboken, NJ, 2009.
(28) Goldstein, M.; Tok, G. C. *J. Chem. Soc. (A)* **1971**, 2303.
(29) Atkins, P.; Overton, T.; Rourke, J.; Weller, M.; Armsrong, F. *Shriver & Atkins Inorganic Chemistry*, 4th ed.; W. H. Freeman and Company: New York, 2006.
(30) Kobayashi, J.; Kushida, T.; Kawashima, T. *J. Am. Chem. Soc.* **2009**, *131*, 10836.
(31) Hitchcock, P. B.; Hu, J.; Lappert, M. F.; Severn, J. R. *Dalton Trans.* **2004**, 4193.
(32) Ding, Y.; Roesky, H. W.; Noltemeyer, M.; Schmidt, H.-G.; Power, P. P. *Organometallics* **2001**, *20*, 1190.
(33) Peng, Y.; Fischer, R. C.; Merrill, W. A.; Fischer, J.; Pu, L.; Ellis, B. D.; Fettinger, J. C.; Herber, R. H.; Power, P. P. *Chem. Sci.* **2010**, *1*, 461.
(34) Sen, S. S.; Kritzler-Kosch, M. P.; Nagendran, S.; Roesky, H. W.; Beck, T.; Pal, A.; Herbst-Irmer, R. *Eur. J. Inorg. Chem.* **2010**, 5304.
(35) Jana, A.; Roesky, H. W.; Schulzke, C.; Döring, A. *Angew. Chem., Int. Ed.* **2009**, *48*, 1106.
(36) Jana, A.; Roesky, H. W.; Schulzke, C.; Samuel, P. P. *Organometallics* **2010**, *29*, 4837.
(37) Nechaev, M. S.; Chernov, O. V.; Portnyagin, I. A.; Khrustalev, V. N.; Aysin, R. R.; Lunin, V. V. *J. Organomet. Chem.* **2010**, *695*, 365.
(38) Wolff, M.; Harmening, T.; Pöttgen, R.; Feldmann, C. *Inorg. Chem.* **2009**, *48*, 3153.
(39) Müller, U.; Mronga, N.; Schumacher, C.; Dehnicke, K. *Z. Naturforsch.* **1982**, *37*, 1122.
(40) Jana, A.; Schwab, G.; Roesky, H. W.; Stalke, D. *Inorg. Chim. Acta* **2010**, *363*, 4408.
(41) Henn, M.; Deáky, V.; Krabbe, S.; Schürmann, M.; Prosenc, M. H.; Herres-Pawlis, S.; Mahieu, B.; Jurkschat, K. *Z. Anorg. Allg. Chem.* **2011**, *637*, 211.
(42) Pacher, A.; Schrenk, C.; Schnepf, A. *J. Organomet. Chem.* **2010**, *695*, 941.
(43) Weinhold, F. In *Encyclopedia of Computational Chemistry*; von Ragué Schleyer, P., Ed.; Wiley: Chichester, U.K., 1998; Vol. 3, p 1792.
(44) Herber, R. H.; Nowik, I. *Phosphorus, Sulfur Silicon Relat. Elem.* **2011**, 1336.
(45) Herber, R. H.; Nowik, I.; Cohen, S. *J. Physics Conf. Series* **2010**, *217*, 012145.
(46) Parak, F.; Knapp, W. *Proc. Natl. Acad. Sci. U.S.A.* **1984**, *81*, 7088.
(47) Parak, F.; Hartmann, H.; Aumann, K. D.; Reuschel, H.; Rennekamp, G.; Bartunik, H.; Steigemann, W. *Eur. Biophys. J.* **1987**, *15*, 237.
(48) Nowik, I.; Bauminger, E. R.; Cohen, S. G.; Ofer, S. *Phys. Rev.* **1985**, *A31*, 2291.
(49) Nowik, I.; Cohen, S. G.; Bauminger, E. R.; Ofer, S. *Phys. Rev.* **1983**, *50*, 1528.
(50) Parak, F.; Formanek, H. *Acta. Crystallogr., Sect. A* **1971**, *27*, 573.
(51) Coddington, J. M.; Taylor, M. J. *J. Chem. Soc., Dalton Trans.* **1989**, 2223.
(52) Lambert, J. B. In *Tin Chemistry: Fundamentals, Frontiers, and Applications*; Davies, A. G., Gielen, M., Pannell, K. H., Tiekink, E. R., Eds.; Wiley: West Sussex, U.K., 2008, p 152.
(53) (a) Ramsey, N. F. *Phys. Rev.* **1950**, *78*, 699. (b) Ramsey, N. F. *Phys. Rev.* **1951**, *83*, 540. (c) Ramsey, N. F. *Phys. Rev.* **1952**, *86*, 243.
(54) Te Velde, G.; Bickelhaupt, F. M.; Baerends, E. J.; Fonseca Guerra, C.; van Gisbergen, S. J. A.; Snijders, J. G.; Ziegler, T. *J. Comput. Chem.* **2001**, *22*, 931.
(55) Frisch, M. J.; Trucks, G. W.; Schlegel, H. B.; Scuseria, G. E.; Robb, M. A.; Cheeseman, J. R.; Scalmani, G.; Barone, V.; Mennucci, B.; Petersson, G. A.; Nakatsuji, H.; Caricato, M.; Li, X.; Hratchian, H. P.; Izmaylov, A. F.; Bloino, J.; Zheng, G.; Sonnenberg, J. L.; Hada, M.; Ehara, M.; Toyota, K.; Fukuda, R.; Hasegawa, J.; Ishida, M.; Nakajima, T.; Honda, Y.; Kitao, O.; Nakai, H.; Vreven, T.; Montgomery, J. J. A.; Peralta, J. E.; Ogliaro, F.; Bearpark, M.; Heyd, J. J.; Brothers, E.; Kudin, K. N.; Staroverov, V. N.; Kobayashi, R.; Normand, J.; Raghavachari, K.; Rendell, A.; Burant, J. C.; Iyengar, S. S.; Tomasi, J.; Cossi, M.; Rega, N.; Millam, N. J.; Klene, M.; Knox, J. E.; Cross, J. B.; Bakken, V.; Adamo, C.; Jaramillo, J.; Gomperts, R.; Stratmann, R. E.; Yazyev, O.; Austin, A. J.; Cammi, R.; Pomelli, C.; Ochterski, J. W.; Martin, R. L.; Morokuma, K.; Zakrzewski, V. G.; Voth, G. A.; Salvador, P.; Dannenberg, J. J.; Dapprich, S.; Daniels, A. D.; Farkas, Ö.; Foresman, J. B.; Ortiz, J. V.; Cioslowski, J.; Fox, D. J. *Gaussian 09*, Revision A1 ed.; Gaussian Inc.: Wallingford, CT, 2009.
(56) Krossing, I.; Raabe, I. *Angew. Chem., Int. Ed.* **2004**, *43*, 2066.
(57) Huang, L.; Huang, X. In *Electronic Encyclopedia of Reagents in Organic Synthesis*; Wiley: New York, 2005; Vol. *226*.
(58) Boersma, A. D.; Goff, H. M. *Inorg. Chem.* **1982**, *21*, 581.
(59) Johnston, D. H.; Shriver, D. F. *Inorg. Chem.* **1993**, *32*, 1045.
(60) Collins, G. S.; Kachnowski, T.; Benczer-Koller, N.; Pasternak, M. *Phys. Rev. B* **1979**, *19*, 1369.
(61) *SMART*; Bruker AXS Inc.: Madison, WI, 2001.
(62) *COLLECT*; Nonius BV: Delft, The Netherlands, 2001.
(63) *SAINTPlus*; Bruker AXS Inc.: Madison, WI, 2001.
(64) *SADABS*; Bruker AXS Inc.: Madison, WI, 2001.
(65) Otwinowski, Z.; Minor, W. In *Macromolecular Crystallography*; Carter, C. W. J., Sweet, R. M., Eds.; Academic Press: New Work, 1997; Vol. Part A, p 307.
(66) Sheldrick, G. M. *Acta. Crystallogr., Sect. A: Found Crystallogr.* **2008**, *64*, 112.
(67) Farrugia, L. J. *J. Appl. Crystallogr.* **1999**, *32*, 837.
(68) Spek, A. L. *J. Appl. Crystallogr.* **2003**, *36*, 7.
(69) Mansell, S. M.; Herber, R. H.; Nowik, I.; Ross, D. H.; Russell, C. A.; Wass, D. F. *Inorg. Chem.* **2011**, *50*, 2252.
(70) MacGregor, A. W.; O'Dell, L. A.; Schurko, R. W. *J. Magn. Reson.* **2011**, *208*, 103.
(71) Eichele, K.; Wasylishen, R. E. *WSolids1: Solid-State NMR Spectrum Simulation*; 2001
(72) Tao, J.; Perdew, J. P.; Staroverov, V. N.; Scuseria, G. E. *Phys. Rev. Lett.* **2003**, *91*, 146401.